ADVANCED FUNCTIONAL MATERIALS
www.afm-journal.de

Controlling Crystallite Orientation of Diketopyrrolopyrrole-Based Small Molecules in Thin Films for Highly Reproducible Multilevel Memory Device: Role of Furan Substitution

*Yang Li, Hua Li, Hongfei Chen, Yu Wan, Najun Li, Qingfeng Xu, Jinghui He, Dongyun Chen, Lihua Wang, and Jianmei Lu**

For the organic memory device with vertically arranged electrodes, controlling the film-packing to achieve highly oriented crystallite arrangement is critical but challenging for obtaining the satisfied performance. Here, the effect of backbone planarity on the crystallite orientation is studied. Two diketopyrrolopyrrole-based small molecules (NI_2PDPP and NI_2FDPP) are synthesized with increasing planarity by furan substitution for phenyl rings. Upon thin-film analysis by atomic force microscopy, X-ray diffraction, and grazing-incidence small-angle X-ray scattering, the orientations of these crystallites are demonstrated to be well controlled through tailoring molecular planarity. The highly planar NI_2FDPP in film prefers out-of-plane crystallite orientation with respect to the substrate normal while the nonplanar NI_2PDPP displays less ordered packing with a broad orientation distribution relative to the substrate. As a result, NI_2FDPP-based memory device exhibits superior multilevel performance. More importantly, the oriented crystallite arrangement favors uniformity in NI_2FDPP thin film, thus, the device displays higher reproducibility of memory effects. This study provides an effective synthetic strategy for designing multilevel memory materials with favorable crystallite orientation.

1. Introduction

In recent years, organic memory devices (OMDs) have attracted considerable attention for their potential application in the field of high-density data storage.[1] In contrast with the conventional binary electronics with downscaling limits,[2] OMDs could realize high-density data storage through multilevel memory effects, leading to a dramatically increasing storage capacity.[3] Despite that small molecules have been demonstrated promising in achieving high-performance binary data storage,[4] multilevel memory devices based on these organic materials remains technologically challenging.[5] Among successful examples, several strategies were employed, including morphology engineering[6] and molecular innovation.[5c,7] However, few methods paid attention to their influence on the internal crystallite orientation, which has proven to be a key role in determining the device performance elsewhere.[8]

The importance of internal crystallite orientation uniformity to device performance is related to the charge transport. Anisotropic charge transport often occurs in the organic semiconducting materials.[9] In poly- or semicrystalline organic thin films, the transport of charge carriers inside the crystalline regions is generally believed much faster than that in amorphous regions or grain boundaries.[8c,10] The crystallite orientation, including the in-plane orientation[11] and crystallite alignment relative to the substrate normal (texture),[12] is significant for influencing the connectivity between crystalline regions, which dictates the charge transport efficiency.[13] Thus, in order to obtain high device performance, the alignment between adjacent crystallites should be optimized for efficient charge transport.[14] For instance, because of the highly textured crystallites nucleated from the buried interface, field-effect mobility of poly(3-hexylthiophene)-based organic thin-film transistors (OTFTs) has been shown to be two orders of magnitude increased.[12]

In this work, we controlled the crystallite orientations of organic thin films by tuning the molecular planarity of diketopyrrolopyrrole (DPP)-based small molecuels. Two molecules (NI_2PDPP and NI_2FDPP, shown in **Figure 1**) were synthesized and fabriacated as the memory devices. The choice of DPP as acceptor arises from its remarkable aggregating properties. DPP moieties have emerged as promising building blocks for high-performing materials in transistors and solar cells.[15] However, diphenyl-DPP-based organic electronics usually suffer from relatively poor charge mobility,[16] due to a torsional twist between the phenyl rings and DPP core.[17] We found that replacing the phenyl groups by furans could attenuate the backbone twist, increase the molecular planarity,[18] and hence significantly improve the orientation alignment of crystallites. Thus, NI_2FDPP-based memory device shows superior

Y. Li, Prof. H. Li, H. Chen, Y. Wan, Prof. N. Li, Prof. Q. Xu, Prof. J. He, Dr. D. Chen, L. Wang, Prof. J. Lu
College of Chemistry
Chemical Engineering and Materials Science
Collaborative Innovation Center of Suzhou Nano Science and Technology
Soochow University
Suzhou 215123, P. R. China
E-mail: lujm@suda.edu.cn

DOI: 10.1002/adfm.201501271

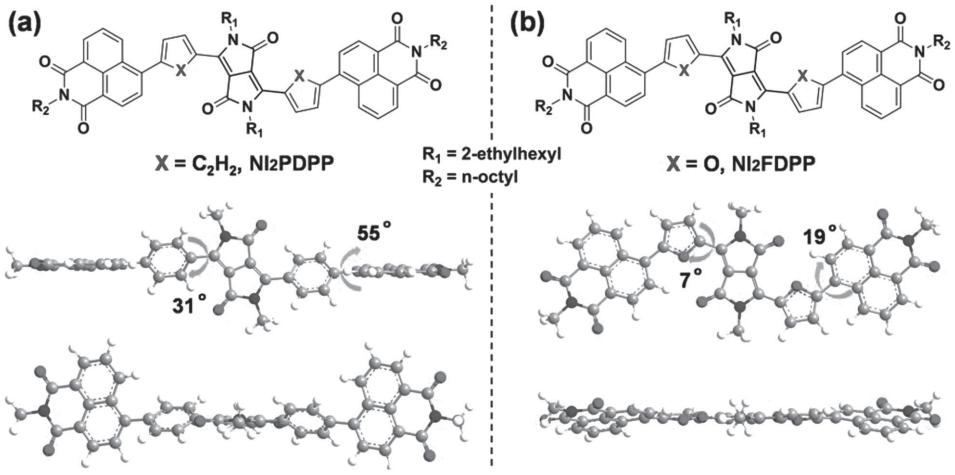

Figure 1. Chemical structures (top) and GGA-predicted (unrestricted BLYP/DNP level) conformations of a) NI_2PDPP and b) NI_2FDPP in front view (middle) and side view (bottom) illustrating the decreased torsional backbone twist.

performance, in particular the low threshold voltages and high reproducible multilevel memory effects.

2. Results and Discussion

2.1. Synthesis and Characterization

NI_2PDPP and NI_2FDPP were synthesized from combining DPP precursors and naphthalimide groups by palladium-catalyzed Suzuki–Miyaura cross-coupling reactions (see the Supporting Information for details). Naphthalimide has also been widely used as acceptor because of the good π-conjugation.[19] The chemical structures of these two compounds were characterized via NMR spectroscopy and high-resolution mass spectrometry. By introducing multiple alkyl chains, NI_2PDPP and NI_2FDPP show good solubility in the most common organic solvents such as $CHCl_3$, toluene, and chlorobenzene.

Thermo gravimetric analysis (TGA) was carried out to examine the thermal stability of these two molecules. NI_2PDPP and NI_2FDPP both exhibit good thermal stability with decomposition temperature (5% weight-loss) to be approximately 296 and 263 °C, respectively, which is conductive to the material longevity (Figure S1, Supporting Information).

2.2. Optical and Electrochemical Properties

The UV–vis absorption spectra were conducted to study the effects of furan substitution on the optical properties of these two DPP-based molecules in solution and thin film (**Figure 2**), and characteristics of the corresponding absorption are summarized in Table S1 in the Supporting Information. In solutions, NI_2PDPP presents a low-energy band from 400 to 550 nm (150 nm), and NI_2FDPP displays a low-energy band from 450 to 700 nm (250 nm), attributed to intramolecular charge transfer (ICT).[20] Furanyl substitution leads to a bathochromic shift for their ICT electronic absorbance. In films, NI_2PDPP shows a λ_{max} at 498 nm and an absorption onset at 564 nm (E_g = 2.20 eV), while NI_2FDPP shows a λ_{max} at 661 nm and an absorption onset at 735 nm (E_g = 1.69 eV). Incorporation of furanyl donors reduces the optical band gap (E_g) by ≈0.5 eV, which may be ascribed to the increased backbone planarity that correlates with the less steric demands of five-membered furan heterocycles. Increased planarity extends effective conjugated length and charge delocalization, thus narrowing the band gap. In addition, NI_2FDPP exhibits a much broader absorption band relative to that in solution and one vibronic shoulder peak is clearly observed, while NI_2PDPP only shows a slight red-shift. These results are probably due to the different formation of molecular aggregates.[21]

The electrochemical properties of NI_2PDPP and NI_2FDPP were characterized by cyclic voltammograms (CVs) (Figure S2, Supporting Information), and are summarized in Table S1 in the Supporting Information as well. The E_{ox}(onset) value of NI_2FDPP tends to be less positive, which indicates a decrease of the (electrochemical) band gap.[22] This trend is in good agreement with the aforementioned optical properties. The highest occupied molecular orbital (HOMO)/lowest unoccupied molecular orbital (LUMO) energy levels of NI_2PDPP and

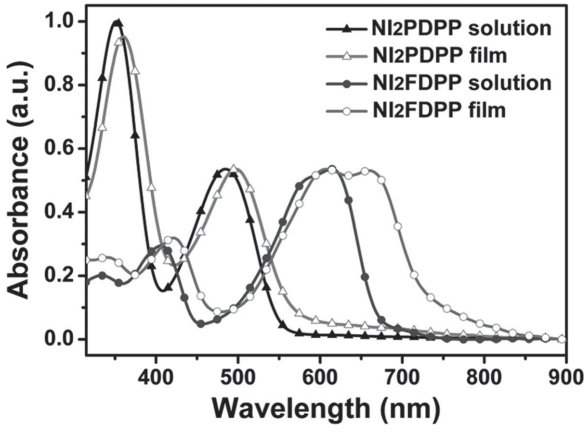

Figure 2. UV–visible absorption spectra of NI2PDPP and NI2FDPP in solution and as thin film on a quartz plate.

NI_2FDPP are determined to be −5.38/−3.18 and −5.19/−3.50 eV, respectively. It can be seen that the HOMO level displays a rise upon the substitution of electron-rich furan for phenyl ring, which approaches the work function of ITO electrode and may facilitate the charge injection.[23]

2.3. Theoretical Calculations

Density functional theory (DFT) calculations were adopted to simulate each molecular backbone of NI_2PDPP and NI_2FDPP. Computation was implemented with generalized gradient approximation (GGA) in DMol3 code, using unrestricted BLYP/DNP level.[24] Both the two molecules show symmetric conformations. It is worth noting that the two molecules have two apparently distinguished geometries. As shown in Figure 1a, the optimized geometry of NI_2PDPP reveals that steric hindrance resulting from the phenyl α-hydrogen atoms and the oxygen atoms of the DPP unit suppresses a coplanar tendency. The hydrogen–oxygen distance is predicted to be 2.46 Å while the sum of the van der Waals radii is 2.61 Å, which suggests an atomic repulsion. The dihedral angle between the phenyl and the DPP unit is found to be 31°. Additionally, an energetic penalty for planarization between the phenyl and the naphthalimide group exists with a dihedral angle of 55°. Contrarily, furan substitution causes increased backbone planarity (Figure 1b). As the furan unit with only one α-hydrogen atom is smaller, steric hindrance between the DPP core and the neighbouring fused ring becomes less. The intramolecular oxygen–oxygen distance from DPP to furan is 2.97 Å, which is comparable to the sum of the van der Waals radii (3.04 Å). Thus, the dihedral angle decreases to 7°. Simultaneously, the repulsion between the furan and the naphthalimide group is also diminished with a dihedral angle of 19°. These calculations reveal that replacing phenyl group with furan allows for a planar structure. Since backbone planarity often benefits π–π interaction and charge transport property, NI_2FDPP-based materials are anticipated to be more promising for OMD application.

2.4. Thin Film Morphology

To examine the effects of structural planarity on microscopic scale morphology, the small-molecule thin films were investigated by atomic force microscopy (AFM) analysis. For sandwich-structured memory devices, films with smooth nanoscale topography are supposed to be beneficial for the efficient charge transport.[25] As depicted in **Figure 3**a, NI_2PDPP forms unevenly aggregated domains in the film. These visible islands are undesirable for OMD films as they can largely impede charge injection with a disordered surface structure (root-mean-square roughness (R_{RMS}) = 6.13 nm, Figure 3c). After the replacement of phenylene rings, these uneven domains disappear and the surface morphology becomes smoother with a roughness of 0.45 nm (Figure 3b,d), forming a well-defined isotropic "granular" structure. This smooth morphology of NI_2FDPP may be ascribed to the backbone coplanarity.[26] The regular thin film can promote the charge-carrier transport between small molecules and electrodes.

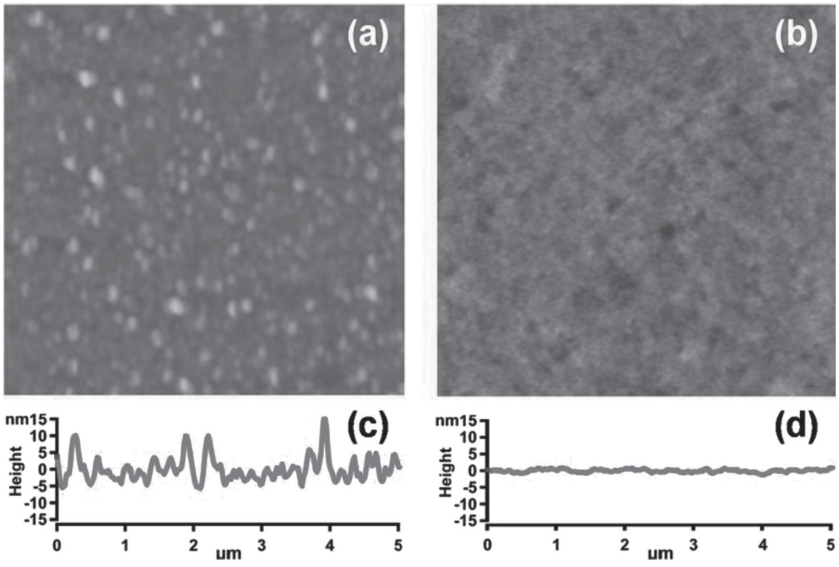

Figure 3. a,b) Morphology characterization of TM-AFM topographic images and c,d) corresponding cross-section profiles of NI_2PDPP and NI_2FDPP films spin-coated on ITO substrates, respectively. The scan size for both images is 5 μm × 5 μm.

2.5. Thin Film Nanostructure

The X-ray diffraction (XRD) analysis was carried out to examine the thin film microstructure, XRD studies reveal the enhancement of molecular ordering after furanyl substitution (Figure S3, Supporting Information). NI_2PDPP shows a primary diffraction peak at $2\theta = 6.3°$, corresponding to a d-spacing of 14.01 Å, which may arise from the crystalline domains observed in AFM image.[27] Another diffraction peak with low intensity also appears at $2\theta = 19.0°$. This weak diffraction can be assigned to the π–π stacking peak with the π–π stacking distance of 4.67 Å.[18a,28] For NI_2FDPP, the intensity of the XRD signals somewhat increases, which likely correlates with the enhanced crystallinity. NI_2FDPP shows an intense primary diffraction peak at $2\theta = 8.2°$ (d = 10.77 Å). This smaller lamellar spacing value is likely originated from a tilted structure or dense packing forms in the film.[29] In particular, one additional diffraction peak is also observed at $2\theta = 24.7°$, corresponding to the π–π stacking distance of 3.60 Å. This π–π stacking peak suggests that there exists strong intermolecular interaction among the donor/acceptor (D–A) conjugated backbone of NI_2FDPP.[30]

Meanwhile, for the thin films, grazing-incidence small-angle X-ray scattering (GISAXS) analysis can be adopted to determine the crystalline properties of films relative to the substrate.[31] As shown in **Figure 4**a, both the two samples (film on substrate) were impinged by the monochromatic X-ray beam respectively with a very small incident angle. GISAXS pattern of NI_2PDPP

shows a sharp ring including a more intense arcing near the q_z plane (Figure 4b). This suggests that the crystallite arrangement in thin film is less ordered, which comprises a broad distribution of orientations relative to the substrate with a slight preference of out-of-plane orientation (Figure 4d).[31a,b] Yet, GISAXS pattern of NI_2FDPP displays an intense elliptic peak along the q_z plane ($q_{xy} = 0$), indicating that NI_2FDPP film is highly oriented that has a preferred out-of-plane crystallite orientation and is isotropic in-plane (a textured film, Figure 4c,e).[31a] Moreover, this scattering peak corresponds to a spacing distance of 10.76 Å, which is very close to the XRD observed lamellar spacing data (10.77 Å). Thus, this pronounced peak along the out-of-plane direction can be assigned to the highly textured lamellar packing peak, implying that the lamellar orientation in thin film is parallel to the substrate.[20,31b] As a result of reduced molecular backbone torsion, the favorable alignment between adjacent crystalline regions is promoted, forming an ordered lamellar packing that relates with good charge transport efficiency.[14a,32] This finding is important since most previous studies about crystallite orientation focused on the effects of processing conditions,[33] solvent,[34] and substrate treatment,[12,35] whereas few studies paid attentions to the π-conjugated backbone structure.

It has been reported that the crystallite orientation alignment with respect to the substrate normal (texture) of films can be tuned by varying side-chain rigidity and thermal history.[36] McCulloch et al. observed that medium C12 side-chain (C10, C12, and C14) based films exhibited an oriented polycrystalline structure after thermal annealing, which was advantageous for charge transport.[36] Yet, according to the observetion in our

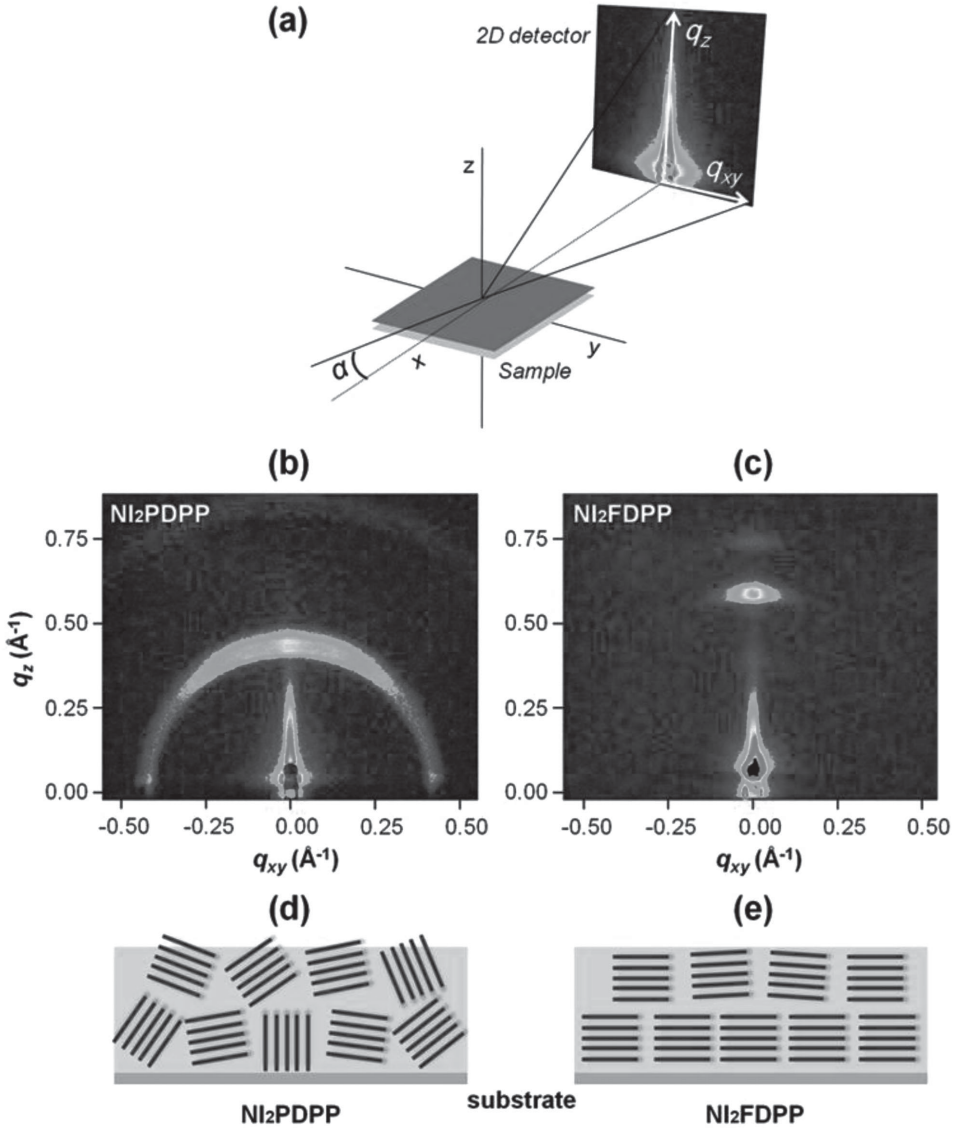

Figure 4. a) Schematic illustration of grazing-incidence small-angle X-ray scattering (GISAXS) with a 2D image plate. The sample was tilted to the incident beam with a glancing angle of $\alpha = 0.20°$. b) GISAXS pattern of NI_2PDPP spun on ITO-coated substrate. c) GISAXS pattern of NI_2FDPP spun on ITO-coated substrate. d) Illustration of nearly random-oriented NI_2PDPP film with a broad crystallite orientation distribution with respect to the substrate normal. e) Illustration of highly oriented NI_2FDPP film with a preferred out-of-plane orientation.

current study, it can be seen that conjugated backbone coplanarity is also capable of influencing the crystallite orientation. Some studies have revealed intermolecular interactions may play a significant role in controlling the thin film growth.[26a,37] In order to understand the effects of molecular planarity on the crystallite orientation, we take these interactions into consideration. For NI_2FDPP, introducing the furan unit contributes to the rigidity and planarity of π-conjugated backbone, which can facilitate the formation of strong cofacial π–π interactions between the small molecules. The strong intermolecular π–π interactions subsequently lead other molecules to grow in a similar face-to-face packing structure, thereby forming a film with ordered orientation. Thus, the highly oriented alignment of crystallites is energetically favored, which warrants the connectivity between crystalline regions. Conversely, for NI_2PDPP, the optimized geometry shows that the naphthalimide side group is nearly perpendicular to the DPP core (Figure 1a). Because of the twisted backbones, the short-distance intermolecular interactions are hindered. Therefore, the energy inducement of favorable crystalline alignment is decreased. In this case, the relatively weak interactions between twisted backbone of NI_2PDPP molecules result in a broad spread of crystalline orientation distribution with respect to the substrate.[38]

2.6. Memory Device Performance

Organic memory devices based on NI_2PDPP and NI_2FDPP were fabricated as ITO/small-molecule/Al sandwich devices and the electrical characteristics were evaluated by current–voltage (*I*–*V*) curves in **Figure 5**. Both the OMDs exhibit ternary memory behavior with different switching threshold voltages (V_{th}s). Notably, V_{th}s trend well with the backbone coplanarity. It is observed that V_{th}s decrease with the reduced molecular torsion. Moreover, the OMDs can be assigned to the typical WORM (write-once, read-many-times) type memory materials according to the following current–voltage sweeps. As shown in Figure 5a, the NI_2PDPP-based device is initially scanned by appling negative voltage (sweep 1). As the voltage increased, two abrupt increases in current are observed at about −1.99 and −2.88 V, respectively, indicating the transition from a low-conductivity (OFF) state to an intermediate-conductivity (ON1) state, and further to higher conductive (ON2) state. This OFF-to-ON1-to-ON2 transition is equivalent to the "writing" process. The high-conductivity state is retained during the subsequent negative scan from 0 to −4.0 V (sweep 2) and positive sweep from 0 to 4 V (sweep 3). By applying a lower negative voltage from 0 to −2.5 V to another cell of the device, the OFF-to-ON1 transition is also induced at about −2.06 V (sweep 4). Subsequent forward and reverse scans from 0 to −2.5 V (sweep 5 and 6) indicate the device remains in its ON1 state. Furthermore, the ON1-to-ON2 transition is obtained in the same cell when approaching a voltage of −3.00 V (sweep 7). The ON2 state could also be maintained for the following negative and positive sweeps (sweep 8 and 9). NI_2FDPP-based device is sequentially investigated and found ternary WORM characteristics as well with two switching threshold voltages (V_{th}s) of –0.98 and –1.77 V (Figure 5b). The current ratio of "OFF," "ON1," and "ON2" states is high, which is crucial for the device to realize

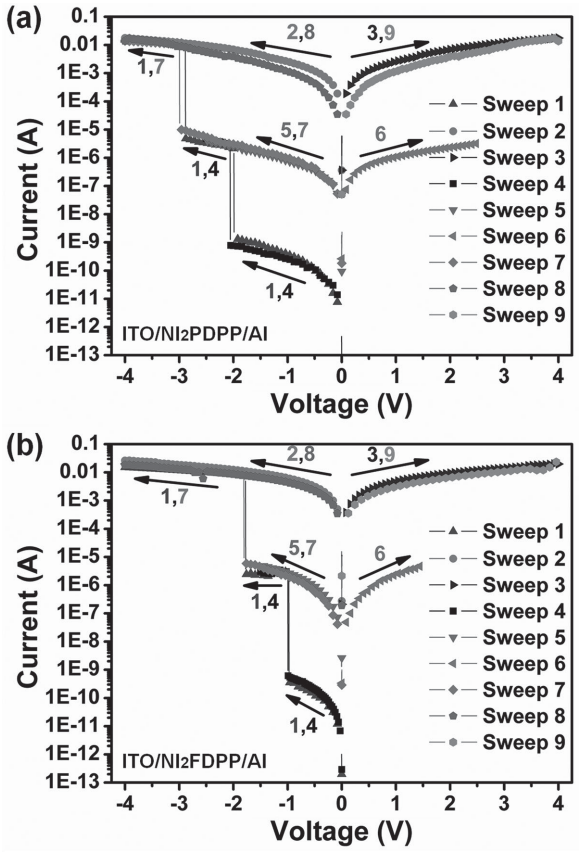

Figure 5. Characteristic current–voltage (*I*–*V*) curves of a) NI2PDPP and b) NI2FDPP based memory devices. Sweep 1–3 are conducted on one cell of the device, and sweep 4–9 are conducted on another cell.

high-resolution and low error memory effect.[39] Furthermore, the stabilities of these two devices are studied by continuous voltage stress and readout test (Figure S4, Supporting Information). During the test, no obvious degradation is observed in any of the three states for at least 10 000 s or one hundred million (10^8) read cycles.

In particular, the V_{th}s of NI_2FDPP-based memory devices are much lower than those of NI_2PDPP-based devices (–0.98 and –1.77 V compared to –1.99 and –2.88 V), which is more promising to realize low power consumption property. This can be attributed to the formation of tight π–π stacking (π-stack distance ≈3.60 Å) in NI_2FDPP film with highly preferred crystallite orientation. In organic semiconductors, the charge transport in two principal transport directions (in the plane of the substrate and along the substrate normal) is usually focused, which demonstrates good correlation with device operation. As the OMDs have vertically arranged electrodes (top Al and bottom ITO), the favorable crystallite arrangement along the substrate normal can align with the direction of principal charge transport and thus induce the superior memory effect with low V_{th}s.

2.7. Memory Device Reproducibility

To further test the effects of crystallite orientation on the memory properties, the reproducibility of the memory device

performance was studied. It is noted that the device based on NI_2FDPP with highly oriented crystallite alignment displays more uniform and reproducible memory effects. We investigated the cell-to-cell uniformity via a statistic on 100 device cells of memory performances from five pieces of ITO substrates. It is found that for NI_2PDPP, only 54% cells show electrical tristability, while for NI_2FDPP, the yield is increased into 71%. Moreover, we compare the distribution of the switching threshold voltages (V_{th}s). As shown in **Figure 6**, the distribution of two V_{th}s in NI_2PDPP-based device is broad. The first threshold voltage ($V_{th}1$) varies from −1.2 to −2.4 V and somewhat mainly distributes between −1.8 and −2.1 V (probability of 60%). The second threshold voltage ($V_{th}2$) varies from −2.5 to −3.7 V and shows no obvious main distribution. However, the distribution of two V_{th}s in NI_2FDPP-based device is apparently narrower than NI_2PDPP. $V_{th}1$ is mostly located between −0.9 and −1.1 V (probability of 83%) and $V_{th}2$ is mostly located between −1.6 and −1.8 V (probability of 68%), which suggests superior reproducibility of memory behavior. Therefore, the significant discrepancies of yields and onset voltages between two types of devices confirm that the multilevel memory performance is indeed enhanced by improving the preferred crystallite orientations of organic thin films.

2.8. Proposed Mechanism of Memory Effect

Some researches have proven that the formation of metal conduction filaments in thin film under high electric field can result in electrical transitions.[40] To investigate the possibility of filament conduction, we introduced a thin layer of LiF (10 nm) between organic active layer and Al electrode, fabricating memory devices with ITO/small-molecule/LiF/Al structure. This layer of LiF is inserted to prevent Al from penetrating into the organic thin film.[41] The electrical characteristics of these fresh memory devices were measured under the same condition (Figure S5, Supporting Information). Notably, the observed electrical switching behavior is similar with that shown in Figure 5, which implies that the switching

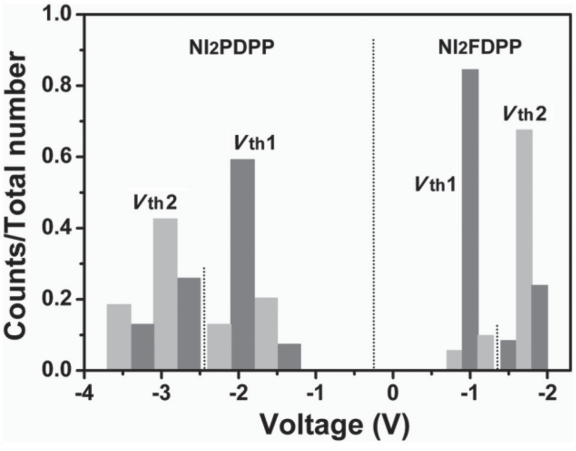

Figure 6. The distribution of switching threshold voltages (V_{th}s) of NI_2PDPP- and NI_2FDPP-based memory devices. $V_{th}1$ represents the first threshold voltage and $V_{th}2$ represents the second one.

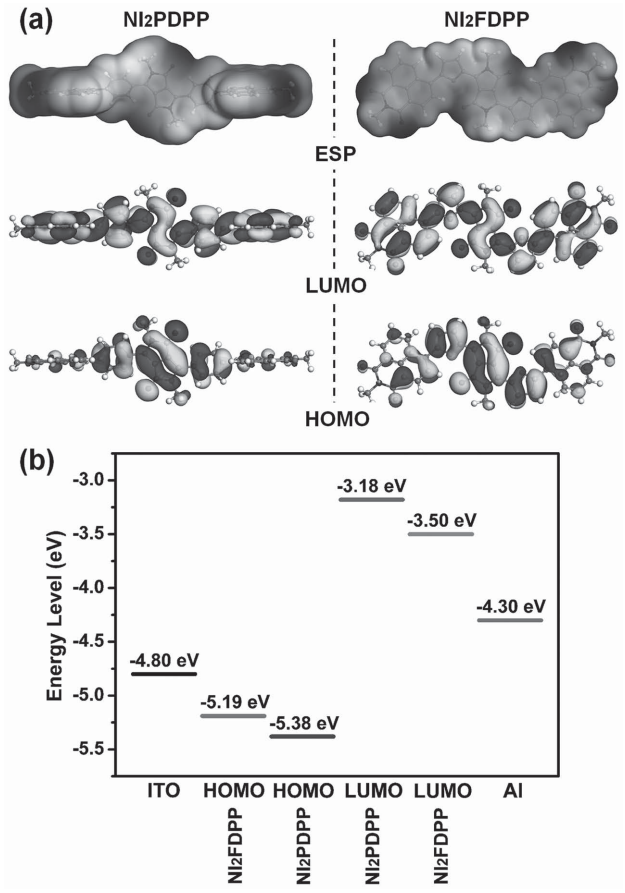

Figure 7. a) DFT molecular simulation results of NI2PDPP and NI2FDPP: molecular electrostatic potential (ESP), HOMO, and LUMO molecular orbitals. b) HOMO and LUMO energy levels diagram for NI2PDPP and NI2FDPP along with the work function of the electrodes (ITO and Al).

phenomenon is independent of the filament conduction. Besides, as the devices exhibit good stability and reproducibility, it can be concluded that the electrical transitions are intrinsic to the organic small molecules rather than the metal filaments.[42]

In order to understand the multilevel memory effects and electronic properties of NI_2PDPP and NI_2FDPP, theoretical calculations were performed via the DFT method. The calculated frontier molecular orbitals and electrostatic potential (ESP) surfaces of these two molecules were shown in **Figure 7**a. It can be noted that the electrons of HOMO orbital mainly locate on the donors while the electrons of LUMO mainly distribute on the electron-deficient acceptors. These electron density distributions of frontier molecular orbitals generally indicate that the intramolecular charge transfer (ICT) process occurs upon undergoing the HOMO to LUMO transition.[6a,43]

Figure 7b illustrates the detailed energy levels of molecular orbitals as well as the work function of electrodes. The hole injection energy barriers between ITO (−4.8 eV) and HOMO are estimated to be 0.58 and 0.39 eV for NI_2PDPP and NI_2FDPP, respectively, which are both smaller than electron injection energy barriers (1.12 and 0.80 eV) between Al (−4.3 eV) and LUMO. This implies that hole injection may dominate the charge conduction process of ITO/small-molecule/Al devices.

In addition, the calculated molecular surface displays continuous positive molecular ESP (in gray white) throughout the conjugated backbone (Figure 7a), which forms an open channel for charge carrier migration. However, negative ESP regions (in black) resulting from the DPP and naphthalimide acceptors also exist. These negative regions could act as "traps" to impede the motion of charge carriers.[25a,44] Under a low negative bias, charge carriers could not get adequate energy to overcome the injection barriers between the donors and acceptors. Thus, the device remains in the OFF state. When the first threshold voltage ($V_{th}1$) is approached, charge carriers gradually get sufficient activation energy and inject from the donors to acceptors. Therefore, the device shows enhanced conductivity and switches from OFF to ON1 state. However, the traps caused by different acceptors may not be filled simultaneously: the trap of DPP is completely filled while the trap of naphthalimide is partly filled. This is probably due to the larger depth of naphthalimide trap, which corresponds to the stronger electron-withdrawing ability of naphthalimide than DPP.[44,45] When applying a higher $V_{th}2$, the accumulated carriers with sufficient injection energy will fill the trap of naphthalimide, leading to a high-conductivity (ON2) state. Thus, the device exhibits multilevel memory effects, attributed to the two charge traps arising from the different electron-withdrawing abilities of naphthalimide and DPP acceptors.[45a] Moreover, the trapped charge carriers could be stabilized by the intra- or intermolecular charge transfer at the excited state, forming a charge-separated state.[44,45b,46] These trapped carriers could not be easily released after removing the power supply or under reverse electric field. Consequently, the resulting high-conductivity state could be long-time maintained, indicating that the device shows WORM memory characteristics.

3. Conclusions

In summary, we have synthesized two DPP-based small molecules with different molecular geometries. DFT calculation shows that the backbone coplanarity is apprently enhanced by replacing phenyl rings with furans. Interestingly, we have found that the highly planar NI_2FDPP induces out-of-plane crystallite alignment in thin film with respect to the substrate normal, while the nonplanar NI_2PDPP displays less ordered packing with a broad distribution of crystallite orientation relative to the substrate. Through molecular planarity modulation, the crystallite orientation is well controlled. The highly preferred crystallite orientation is essential for the small molecule-based OMDs to obtain efficient multilevel memory performance (e.g., low energy consumption). In addition, this oriented arrangement favors uniformity in thin film, and thus, produces OMDs with good stability and reproducibility of memory effects. These findings reveal that high-performing π-conjugated materials can be achieved by strategic design of solid-state properties.

4. Experimental Section

Device Fabrication and Characterization: The memory devices based on the two small molecules were prepared on indium-tin-oxide (ITO)-coated glass substrates. The ITO-coated glass substrates were precleaned with soap water and ultrasonicated for 20 min each in water, acetone, and ethanol sequentially. NI_2PDPP and NI_2FDPP solutions were prepared in chlorobenzene respectively at a concentration of 10 mg mL^{-1} and ultrasonicated for complete dissolution. After filtering through 0.22 μm pore size of syringe filter, the filtrates were spin-coated onto each substrate at a speed of 300 RPM for 6 s, followed by 1500 RPM for 30 s to form thin films on the ITO-coated glass substrates. Finally, the top Al electrodes of about 100 nm in thickness were thermally evaporated and deposited onto the organic layer surface at about 10^{-6} Torr through a shadow mask with circular patterns. The active area of the memory device cell was 0.126 mm^2 (a nummular Al spot with radius of 0.2 mm). Under ambient air condition, the *I–V* measurements of the devices were characterized by a HP 4145B semiconductor parameter analyzer equipped with a HP 8110A pulse generator.

Supporting Information

Supporting Information is available from the Wiley Online Library or from the author.

Acknowledgements

This work was financially supported by the NSF of China (21176164, 21206102, 21336005, and 21476152), the NSF of Jiangsu Province (BE2013052), a project supported by the Specialized Research Fund for the Doctoral Program of Higher Education of China (Grant No. 20123201120005), Chinese-Singapore Joint Project (2012DFG41900), and National Excellent Doctoral Dissertation funds (201455). The authors thank Prof. Xiaofang Chen and Mr. Feng Zhang from Soochow University for helpful discussion about the X-ray scattering.

Received: March 30, 2015
Published online: May 29, 2015

[1] a) J. Liu, Z. Yin, X. Cao, F. Zhao, L. Wang, W. Huang, H. Zhang, *Adv. Mater.* **2013**, *25*, 233; b) Q.-D. Ling, D.-J. Liaw, C. Zhu, D. S.-H. Chan, E.-T. Kang, K.-G. Neoh, *Prog. Polym. Sci.* **2008**, *33*, 917; c) J. C. Scott, L. D. Bozano, *Adv. Mater.* **2007**, *19*, 1452; d) B.-B. Cui, Z. Mao, Y. Chen, Y.-W. Zhong, G. Yu, C. Zhan, J. Yao, *Chem. Sci.* **2015**, *6*, 1308; e) T. Sekitani, T. Yokota, U. Zschieschang, H. Klauk, S. Bauer, K. Takeuchi, M. Takamiya, T. Sakurai, T. Someya, *Science* **2009**, *326*, 1516; f) J. E. Green, J. W. Choi, A. Boukai, Y. Bunimovich, E. Johnston-Halperlin, E. Delonno, Y. Luo, B. A. Sheriff, K. Xu, Y. S. Shin, H.-R. Tseng, J. F. Stoddart, J. R. Heath, *Nature* **2007**, *445*, 414.

[2] a) R. Chau, B. Doyle, S. Datta, J. Kavalieros, K. Zhang, *Nat. Mater.* **2007**, *6*, 810; b) Y. Jung, S.-H. Lee, A. T. Jennings, R. Agarwal, *Nano Lett.* **2008**, *8*, 2056.

[3] a) J.-S. Lee, Y.-M. Kim, J.-H. Kwon, J. S. Sim, H. Shin, B.-H. Sohn, Q. Jia, *Adv. Mater.* **2011**, *23*, 2064; b) C. Simao, M. Mas-Torrent, J. Casado-Montenegro, F. Oton, J. Veciana, C. Rovira, *J. Am. Chem. Soc.* **2011**, *133*, 13256.

[4] a) J. Lee, E. Lee, S. Kim, G. S. Bang, D. A. Shultz, R. D. Schmidt, M. D. E. Forbes, H. Lee, *Angew. Chem. Int. Ed.* **2011**, *50*, 1; b) R. C. G. Naber, K. Asadi, P. W. M. Blom, D. M. de Leeuw, B. De Boer, *Adv. Mater.* **2010**, *22*, 933; c) C. P. Collier, G. Mattersteig, E. W. Wong, Y. Luo, K. Beverly, J. Sampaio, F. M. Raymo, J. F. Stoddart, J. R. Heath, *Science* **2000**, *289*, 1172.

[5] a) C. Ye, Q. Peng, M. Li, J. Luo, Z. Tang, J. Pei, J. Chen, Z. Shuai, L. Jiang, Y. Song, *J. Am. Chem. Soc.* **2012**, *134*, 20053; b) T. Lee,

S.-U. Min, J. Kim, J.-W. Choi, *Adv. Mater.* **2010**, *22*, 510; c) H. Li, Q. Xu, N. Li, R. Sun, J. Ge, J. Lu, H. Gu, F. Yan, *J. Am. Chem. Soc.* **2010**, *132*, 5542.

[6] a) W.-Y. Lee, T. Kurosawa, S.-T. Lin, T. Higashihara, M. Ueda, W.-C. Chen, *Chem. Mater.* **2011**, *23*, 4487; b) S. Miao, H. Li, Q. Xu, N. Li, J. Zheng, R. Sun, J. Lu, C. M. Li, *J. Mater. Chem.* **2012**, *22*, 16582.

[7] a) A. J. Kronemeijer, H. B. Akkerman, T. Kudernac, B. J. van Wees, B. L. Feringa, P. W. M. Blom, B. de Boer, *Adv. Mater.* **2008**, *20*, 1467; b) M. J. Rozenberg, I. H. Inoue, M. J. Sánchez, *Phys. Rev. Lett.* **2004**, *92*, 178302.

[8] Methods of influencing small molecule packing orientation in thin film: a) V. S. Gevaerts, E. M. Herzig, M. Kirkus, K. H. Hendriks, M. M. Wienk, J. Perlich, P. Müller-Buschbaum, R. A. J. Janssen, *Chem. Mater.* **2014**, *26*, 916; b) S. C. B. Mannsfeld, M. L. Tang, Z. Bao, *Adv. Mater.* **2011**, *23*, 127; c) J. Rivnay, L. H. Jimison, J. E. Northrup, M. F. Toney, R. Noriega, S. Lu, T. J. Marks, A. Facchetti, A. Salleo, *Nat. Mater.* **2009**, *8*, 952.

[9] a) V. Coropceanu, J. Cornil, D. A. da Silva Filho, Y. Olivier, R. Silbey, J.-L. Brédas, *Chem. Rev.* **2007**, *107*, 926; b) J. L. Bredas, D. Beljonne, V. Coropceanu, J. Cornil, *Chem. Rev.* **2004**, *104*, 4971.

[10] a) W. H. Lee, D. H. Kim, Y. Jang, J. H. Cho, M. Hwang, Y. D. Park, Y. H. Kim, J. I. Han, K. Cho, *Appl. Phys. Lett.* **2007**, *90*, 132106; b) R. L. Headrick, S. Wo, F. Sansoz, J. E. Anthony, *Appl. Phys. Lett.* **2008**, *92*, 063302; c) H. E. Katz, *Chem. Mater.* **2004**, *16*, 4748.

[11] a) E. Cho, C. Risko, D. Kim, R. Gysel, N. Cates Miller, D. W. Breiby, M. D. McGehee, M. F. Toney, R. J. Kline, J.-L. Bredas, *J. Am. Chem. Soc.* **2012**, *134*, 6177; b) V. Kalihari, E. B. Tadmor, G. Haugstad, C. D. Frisbie, *Adv. Mater.* **2008**, *20*, 4033.

[12] R. J. Kline, M. D. McGehee, M. F. Toney, *Nat. Mater.* **2006**, *5*, 222.

[13] a) R. A. Street, J. E. Northrup, A. Salleo, *Phys. Rev. B* **2005**, *71*, 165202; b) A. Salleo, T. W. Chen, A. R. Völkel, Y. Wu, P. Liu, B. S. Ong, R. A. Street, *Phys. Rev. B* **2004**, *70*, 115311.

[14] a) E. Verploegen, R. Mondal, C. J. Bettinger, S. Sok, M. F. Toney, Z. Bao, *Adv. Funct. Mater.* **2010**, *20*, 3519; b) D. M. DeLongchamp, R. J. Kline, E. K. Lin, D. A. Fischer, L. J. Richter, L. A. Lucas, M. Heeney, I. McCulloch, J. E. Northrup, *Adv. Mater.* **2007**, *19*, 833; c) H. Sirringhaus, P. J. Brown, R. H. Friend, M. M. Nielsen, K. Bechgaard, B. M. W. Langeveld-Voss, A. J. H. Spiering, R. A. J. Janssen, E. W. Meijer, P. Herwig, D. M. de Leeuw, *Nature* **1999**, *401*, 685.

[15] a) H.-J. Yun, S.-J. Kang, Y. Xu, S. O. Kim, Y.-H. Kim, Y.-Y. Noh, S.-K. Kwon, *Adv. Mater.* **2014**, *26*, 7300; b) J. Jo, J.-R. Pouliot, D. W, S. D. Collins, J. Y. Kim, T. L. Nguyen, H. Y. Woo, Y. Sun, M. Leclerc, A. J. Heeger, *Adv. Mater.* **2013**, *25*, 4783; c) W. Li, K. H. Hendriks, A. Furlan, W. S. C. Roelofs, M. M. Wienk, R. A. J. Janssen, *J. Am. Chem. Soc.* **2013**, *135*, 18942; d) Y. Li, P. Sonar, L. Murphy, W. Hong, *Energy Environ. Sci.* **2013**, *6*, 1684; e) S. Qu, H. Tian, *Chem. Commun.* **2012**, *48*, 3039; f) L. Dou, J. Gao, E. Richard, J. You, C.-C. Chen, K. C. Cha, Y. He, G. Li, Y. Yang, *J. Am. Chem. Soc.* **2012**, *134*, 10071.

[16] a) C. M. Proctor, J. A. Love, T.-Q. Nguyen, *Adv. Mater.* **2014**, *26*, 5957; b) P.-T. Wu, F. S. Kim, S. A. Jenekhe, *Chem. Mater.* **2011**, *23*, 4618.

[17] C. Kim, J. Liu, J. Lin, A. B. Tamayo, B. Walker, G. Wu, T.-Q. Nguyen, *Chem. Mater.* **2012**, *24*, 1699.

[18] a) C. B. Nielsen, M. Turbiez, I. McCulloch, *Adv. Mater.* **2013**, *25*, 1859; b) Y. Li, P. Sonar, S. P. Singh, W. Zeng, M. S. Soh, *J. Mater. Chem.* **2011**, *21*, 10829.

[19] Z. Liu, G. Zhang, Z. Cai, X. Chen, H. Luo, Y. Li, J. Wang, D. Zhang, *Adv. Mater.* **2014**, *26*, 6965.

[20] T. L. Nelson, T. M. Young, J. Liu, S. P. Mishra, J. A. Belot, C. L. Balliet, A. E. Javier, T. Kowalewski, R. D. McCullough, *Adv. Mater.* **2010**, *22*, 4617.

[21] a) J. Liu, Y. Sun, P. Moonsin, M. Kuik, C. M. Proctor, J. Lin, B. B. Hsu, V. Promarak, A. J. Heeger, T.-Q. Nguyen, *Adv. Mater.* **2013**, *25*, 5898; b) H. Bronstein, Z. Chen, R. S. Ashraf, W. Zhang, J. Du Durrant, J. R. P. S. Tuladhar, K. Song, S. E. Watkins, Y. Geerts, M. M. Wienk, R. A. J. Janssen, T. Anthopoulos, H. Sirringhaus, M. Heeney, I. McCulloch, *J. Am. Chem. Soc.* **2011**, *133*, 3272.

[22] M-H. Yoon, A. Facchetti, C. E. Stern, T. J. Marks, *J. Am. Chem. Soc.* **2006**, *128*, 5792.

[23] Z. Yi, L. Ma, B. Chen, D. Chen, X. Chen, J. Qin, X. Zhan, Y. Liu, W. Ong, J. Li, *Chem. Mater.* **2013**, *25*, 4290.

[24] B. Delley, *J. Chem. Phys.* **2000**, *113*, 7756.

[25] a) X.-D. Zhuang, Y. Chen, G. Liu, B. Zhang, K.-G. Neoh, E.-T. Kang, C.-X. Zhu, Y.-X. Li, L.-J. Niu, *Adv. Funct. Mater.* **2010**, *20*, 2916; b) S.-L. Lian, C.-L. Liu, W.-C. Chen, *ACS Appl. Mater. Interfaces* **2011**, *3*, 4504; c) S. G. Hahm, S. Choi, S.-H. Hong, T. J. Lee, S. Park, D. M. Kim, W.-S. Kwon, K. Kim, O. Kim, M. Ree, *Adv. Funct. Mater.* **2008**, *18*, 3276.

[26] a) M. S. Chen, J. R. Niskala, D. A. Unruh, C. K. Chu, O. P. Lee, J. M. J. Fréchet, *Chem. Mater.* **2013**, *25*, 4088; b) J. Liu, B. Walker, A. Tamayo, Y. Zhang, T.-Q. Nguyen, *Adv. Funct. Mater.* **2013**, *23*, 47.

[27] W. Shin, T. Yasuda, G. Watanabe, Y. S. Yang, C. Adachi, *Chem. Mater.* **2013**, *25*, 2549.

[28] N. Allard, R. B. Aich, D. Gendron, P.-L. T. Boudreault, C. Tessier, S. Alem, S.-C. Tse, Y. Tao, M. Leclerc, *Macromolecules* **2010**, *43*, 2328.

[29] a) H. Usta, C. Newman, Z. Chen, A. Facchetti, *Adv. Mater.* **2012**, *24*, 3678; b) J. S. Lee, S. K. Son, S. Song, H. Kim, D. R. Lee, K. Kim, M. J. Ko, D. H. Choi, B. Kim, J. H. Cho, *Chem. Mater.* **2012**, *24*, 1316; c) Y. Zhang, C. Kim, J. Lin, T.-Q. Nguyen, *Adv. Funct. Mater.* **2012**, *22*, 97.

[30] a) Y. Li, P. Sonar, S. P. Singh, M. S. Soh, M. van Meurs, J. Tan, *J. Am. Chem. Soc.* **2011**, *133*, 2198; b) J. S. Ha, K. H. Kim, D. H. Choi, *J. Am. Chem. Soc.* **2011**, *133*, 10364.

[31] a) J. Rivnay, S. C. B. Mannsfeld, C. E. Miller, A. Salleo, M. F. Toney, *Chem. Rev.* **2012**, *112*, 5488; b) D. M. DeLongchamp, R. J. Kline, D. A. Fischer, L. J. Richter, M. F. Toney, *Adv. Mater.* **2011**, *23*, 319; c) S. Park, K. Kim, D. M. Kim, W. Kwon, J. Choi, M. Ree, *ACS Appl. Mater. Interfaces* **2011**, *3*, 765.

[32] J. Rivnay, R. Steyrleuthner, L. H. Jimison, A. Casadei, Z. H. Chen, M. F. Toney, A. Facchetti, D. Neher, A. Salleo, *Macromolecules* **2011**, *44*, 5246.

[33] a) G. Giri, E. Verploegen, S. C. B. Mannsfeld, S. Atahan-Evrenk, D. H. Kim, S. Y. Lee, H. A. Becerril, A. Aspuru-Guzik, M. F. Toney, Z. Bao, *Nature* **2011**, *480*, 504; b) B. O'Connor, R. J. Kline, B. R. Conrad, L. J. Richter, D. Gundlach, M. F. Toney, D. M. DeLongchamp, *Adv. Funct. Mater.* **2011**, *21*, 3697; c) H. N. Tsao, D. Cho, J. W. Andreasen, A. Rouhanipour, D. W. Breiby, W. Pisula, K. Müllen, *Adv. Mater.* **2009**, *21*, 209.

[34] a) H.-Y. Chen, H. Yang, G. Yang, S. Sista, R. Zadoyan, G. Li, Y. Yang, *J. Phys. Chem. C* **2009**, *113*, 7946; b) R. J. Kline, M. D. McGehee, E. N. Kadnikova, J. Liu, J. M. J. Fréchet, M. F. Toney, *Macromolecules* **2005**, *38*, 3312.

[35] a) L. Qiu, J. A. Lim, X. Wang, W. H. Lee, M. Hwang, K. Cho, *Adv. Mater.* **2008**, *20*, 1141; b) J. Veres, S. Ogier, G. Lloyd, D. de Leeuw, *Chem. Mater.* **2004**, *16*, 4543.

[36] I. McCulloch, M. Heeney, C. Bailey, K. Genevicius, I. MacDonald, M. Shkunov, D. Sparrowe, S. Tierney, R. Wagner, W. Zhang, M. L. Chabinyc, R. J. Kline, M. D. McGehee, M. F. Toney, *Nat. Mater.* **2006**, *5*, 328.

[37] a) W. Chen, D.-C. Qi, H. Huang, X. Gao, A. T. S. Wee, *Adv. Funct. Mater.* **2011**, *21*, 410; b) S. Sergeyev, W. Pisula, Y. H. Geerts, *Chem. Soc. Rev.* **2007**, *36*, 1902.

[38] C. Kanimozhi, M. Naik, N. Y. Gross, E. K. Burnett, A. L. Briseno, T. D. Anthopoulos, S. Patil, *J. Phys. Chem. A.* **2014**, *118*, 11536.

[39] a) Q. D. Ling, F. C. Chang, Y. Song, C. X. Zhu, D. J. Liaw, D. S. H. Chan, E. T. Kang, K. G. Neoh, *J. Am. Chem. Soc.* **2006**, *128*, 8732; b) J. He, L. P. Ma, J. H. Wu, Y. Yang, *J. Appl. Phys.* **2005**, *97*, 064507.

[40] a) W.-P. Lin, S.-J. Liu, T. Gong, Q. Zhao, W. Huang, *Adv. Mater.* **2014**, *26*, 570; b) W.-J. Joo, T.-L. Choi, K.-H. Lee, Y. Chung, *J. Phys. Chem. B* **2007**, *111*, 7756.

[41] a) Z. Liu, E. Shi, Y. Wan, N. Li, D. Chen, Q. Xu, H. Li, J. Lu, K. Zhang, L. Wang, *J. Mater. Chem. C* **2015**, *3*, 2033; b) G. Wang, S. Miao, Q. Zhang, H. Liu, H. Li, N. Li, Q. Xu, J. Lu, L. Wang, *Chem. Commun.* **2013**, *49*, 9470; c) S. M. Yoon, S. H. Yang, S. W. Jung, C. W. Byun, S. H. Park, C. S. Hwang, G. G. Lee, H. Ishiwara, *Appl. Phys. Lett.* **2010**, *96*, 232903.

[42] S. L. Lim, N.-J. Li, J.-M. Lu, Q.-D. Ling, C. X. Zhu, E.-T. Kang, K. G. Neoh, *ACS Appl. Mater. Interfaces* **2009**, *1*, 60.

[43] J. A. Marsden, J. J. Miller, L. D. Shirtcliff, M. M. Haley, *J. Am. Chem. Soc.* **2005**, *127*, 2464.

[44] Q.-D. Ling, Y. Song, S.-L. Lim, E. Y.-H. Teo, Y.-P. Tan, C. Zhu, D. S. H. Chan, D.-L. Kwong, E.-T. Kang, K.-G. Neoh, *Angew. Chem. Int. Ed.* **2006**, *45*, 2947.

[45] a) P. Gu, F. Zhou, J. Gao, G. Li, C. Wang, Q. Xu, Q. Zhang, J. Lu, *J. Am. Chem. Soc.* **2013**, *135*, 14086; b) S. Miao, H. Li, Q. Xu, Y. Li, S. Ji, N. Li, L. Wang, J. Zheng, J. Lu, *Adv. Mater.* **2012**, *24*, 6210.

[46] a) A.-D. Yu, T. Kurosawa, Y.-H. Chou, K. Aoyagi, Y. Shoji, T. Higashihara, M. Ueda, C.-L. Liu, W.-C. Chen, *ACS Appl. Mater. Interfaces* **2013**, *5*, 4921; b) Y. Ma, X. Cao, G. Li, Y. Wen, Y. Yang, J. Wang, S. Du, L. Yang, H. Gao, Y. Song, *Adv. Funct. Mater.* **2010**, *20*, 803.